Chinese Chemical Letters 34 (2023) 108095

Contents lists available at ScienceDirect

Chinese Chemical Letters

journal homepage: www.elsevier.com/locate/cclet

Folic acid-based supramolecules for enhanced stability in potassium ion batteries

Yanan Wang[a,b], Dandan Ouyang[a], Liuqian Yang[a,b], Chunyan Wang[a,b], Jian Sun[c], Hui Zhu[a,*], Jiao Yin[a,*]

[a] Laboratory of Environmental Sciences and Technology, Xinjiang Technical Institute of Physics & Chemistry, and Key Laboratory of Functional Materials and Devices for Special Environments, Chinese Academy of Sciences, Urumqi 830000, China
[b] Center of Materials Science and Optoelectronics Engineering, University of Chinese Academy of Sciences, Beijing 100049, China
[c] Changchun Institute of Applied Chemistry, Chinese Academy of Science, Changchun 130022, China

ARTICLE INFO

Article history:
Received 4 November 2022
Revised 9 December 2022
Accepted 22 December 2022
Available online 24 December 2022

Keywords:
Supramolecules
Hydrogen bond
Solubility
Potassium-ion battery
Anode

ABSTRACT

Organics present significant prospects as environmentally friendly and sustainable electrode materials for potassium ion batteries (PIBs) because of their abundant, recyclable and highly customizable characteristics. However, small molecular organics are easily solubilized in organic electrolytes, resulting in a low capacity and poor stability. Herein, the folic acid-based supermolecules (SM-FAs) are successfully prepared by a hydrothermal assisted self-assembly strategy. Due to multi-locus hydrogen bonds (HBs) and the cyclized π-conjugated interactions, the structural stability of SM-FAs has been significantly improved, and the solubility in carbonate electrolytes has been effectively inhibited. As an anode for PIB, the SM-FA-6 sample exhibits a large capacity (206 mAh/g at 50 mA/g) and an outstanding cycle stability (capacity retention of 91% after 1000 cycles at 50 mA/g). More impressively, an integrative storage mechanism which combines both the general enolization reaction between C=O groups and K^+, and the atypical π–K^+ interaction within the assembled conjugation framework, is unraveled for potassium ion accumulation. It is envisioned that this facile self-assemble strategy opens up a promising avenue to modulate the stability of small molecular organic electrodes with enhanced storage capacity.

Recently, potassium-ion batteries (PIBs) have been considered as a new type of energy storage system, since the resource richness of potassium element and the similar storage mechanism with lithium-ion batteries (LIBs) [1,2]. However, the conventional inorganic intercalation electrode materials, such as graphite and transition metal compounds, fail to inherit their high performance in LIBs when applied to PIBs, which is mainly caused by the larger ionic radius of the K^+ (1.38 Å) in comparison with that of the Li^+ (0.76 Å) [3,4]. The larger size of K^+ often leads to the large volume changes and structural destruction in these intercalation materials during potassium storage, which results in lower capacity and poor cyclic stability [5]. Meanwhile, these inorganic insertion materials tend to be environmentally unfriendly, complex and pricey to extract and synthesize, as well as facing a shortage of resources [6]. Therefore, it is urgent to develop functional anode materials that can accommodate large radius K^+ while realizing environmental friendliness applications.

Organic materials, especially those derived from nature and biomass, are recently considered as one of the prospecting electrode materials in batteries owing to their several merits such as sustainability and degradability. More importantly, organic materials generally present more flexible molecular structures, which is more advantageous to effectively solve these problems such as serious volume expansion caused by the insertion of larger K^+ [7]. However, for the practice of organic electrodes, the most prominent problem is the terrible dissolution of active materials in electrolytes, suffering from unsatisfactory specific capacity and cycling lifespan [8]. Until now, diverse strategies have been proposed to address this issue, including the loading of organics into porous carbons [9], the utilization of special electrolyte (solid [10] or saturated [11]), and the synthesis of polymers [12]. Most impressively, along with the success in the field of molecule assemble, various kinds of intermolecular forces (covalent force [13], coordination interaction [13,14], extended noncovalent interaction [15] and *etc.*) can be introduced to further suppress the dissolution issue. Among the above-mentioned intermolecular forces, noncovalent interactions such as hydrogen bond (HB) [16] and electro-

* Corresponding authors.
E-mail addresses: huizhu@ms.xjb.ac.cn (H. Zhu), yinjiao@ms.xjb.ac.cn (J. Yin).

https://doi.org/10.1016/j.cclet.2022.108095
1001-8417/

static force [17] can be adopted as effective strategies to construct supramolecules. For instance, it has been discovered that these organic groups (*e.g.*, containing carboxylic acid or amine functional groups) can be utilized to build stable structure by self-assembly of HBs [18]. Unfortunately, their potential application in electrochemical energy storage is difficult to realize due to the fact that the weaker hydrogen bonds in common organic electrolytes tend to be broken [19]. Hence, establishing chemically stable structures to withstand the harsh interactions from electrolytes remains a challenging task, which needs to design linking units based on multi-locus HBs. In addition, the ion storage mechanism underlying is still elusive and needs further elucidation [20].

Inspired by these, the present work takes advantage of the multi-locus HBs of the pteridine groups of the folic acid (FA) molecule to self-assemble in a hydro-alcoholic solvent by the hydrothermal method to construct the chemically stable supramolecule with smectic structure (SM-FA). Due to multi-locus HBs and cyclized π-conjugated interactions, the structural stability of SM-FA can be effectively improved, and the solubility of FA in organic carbonate electrolytes can be efficiently inhibited. As an anode electrode of PIBs, SM-FA-6 exhibits an excellent capacity (206 mAh/g at 50 mA/g) and an outstanding cyclic stability (capacity retention of 91% after 1000 cycles at 50 mA/g). Furthermore, *ex-situ* XPS investigation uncovers that besides the inherited C=O group that can interact with K^+ *via* the enolization reaction, the π-cation interaction within the pteridine units provides the additional adsorptive sites for K^+ storage.

Figs. 1a and b and Fig. S1 (Supporting information) depicts the scanning electron microscopy (SEM) images of the pristine FA and the SM-FA-x (x = 1–7) formed at different hydro-alcoholic ratios. The pristine FA exhibits micron-sized bulk structures, while SM-FAs formed at different hydro-alcoholic ratios differ greatly in morphology. In the water-dominated system, the SM-FA-x (x = 1–4) appeared as flakes, and these nanosheets gradually became thinner with the increase of ethanol. With more than half of ethanol, such as SM-FA-5 and SM-FA-6, these nanosheets with smooth surfaces tend to form flower-like shapes (Fig. 1a and Fig. S1e). While the SM-FA-7 prepared in ethanol shows a net-like structure (Fig. S1h). To investigate the formation mechanism of SM-FA-x, the Fourier transform infrared (FT-IR) spectra were recorded (Fig. 1c and Fig. S3 in Supporting information). The pristine FA exhibits two characteristic peaks of N–H stretched vibrations at 3550 cm^{-1} and 3320 cm^{-1}, which represent the presence of the free -NH_2 terminal groups on the pteridine groups [21]. Nevertheless, as SM-FAs, both of these two peaks disappeared and were replaced by two sets of new peaks. The new peak at 2785 cm^{-1} can be assigned to the O–H stretching vibration of N–H···O, and another set of new peaks at 3227 and 3041 cm^{-1} can be assigned to the N–H stretched vibration of N–H···N [22]. Thus, it can be confirmed that SM-FAs are assembled by HBs between the pteridine groups in FA. The pteridine group is a nitrogen-rich heterocycle with two sets of complementary HB sites [23]. Therefore, there are two modes of HBs assembly in the FA molecule, which are the band HB mode and the disk HB mode (Fig. S2 in Supporting information) [24].

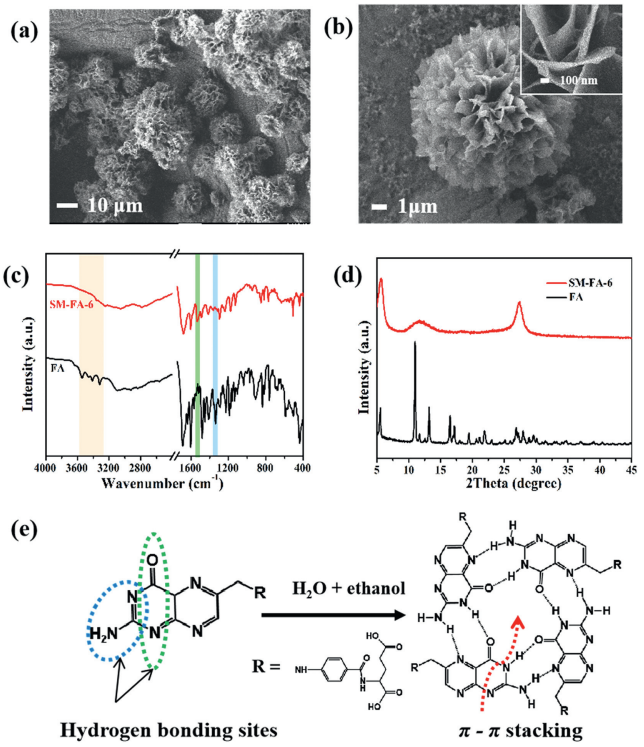

Fig. 1. (a, b) SEM images of SM-FA-6, (c) FT-IR and (d) XRD of FA and SM-FA-6. (e) Synthesis route of SM-FA-x (x = 5–7).

To further investigate the assembly behavior of FA molecules in water and ethanol, SM-FAs were subjected to X-ray diffraction (XRD) analysis (Fig. 1d and Fig. S4 in Supporting information). Compared to the sharp crystal diffraction peaks of the pristine FA, the characteristic peaks of the products after hydrothermal assembly are broadened. This indicates that the assembled SM-FA-x (x = 1–7) possess near-crystalline structure. Furthermore, SM-FA-x (x = 1–4) and SM-FA-x (x = 5–7) present different characteristic peaks, which indicates that they have different structures. It was found that SM-FA-x (x = 1–4) have three main characteristic peaks at 15.1°, 18.5° and 22.4°, representing (100), (110) and (200) crystal planes respectively, signifying that they are ascribed to smectic layered phases. While the characteristic peaks of SM-FA-x (x = 5–7) are located at 5.66°, 11.63° and 27.39°, corresponding to (100), (110) and (001) crystal planes respectively, implying that they belong to hexagonal columnar phases [20]. This may be attributed to the different near-crystalline structures arising from different HB assembly modes [25]. The SM-FA-x (x = 1–4) connected by the band hydrogen bond mode may be smectic layered phases, and the SM-FA-x (x = 5–7) connected by the disk hydrogen bond mode may be hexagonal columnar phases. Moreover, the porosity and the specific surface area of samples were testified by the N_2 adsorption-desorption isotherms. (Fig. S5 and Table S1 in Supporting information). For example, the surface areas of SM-FA-5, SM-FA-6 and SM-FA-7 are 89, 154 and 319 m^2/g, respectively. As shown in Fig. 1e, upon the addition of ethanol into water, the polarity of the solvent is modulated, which affects the solubility and the ionic states of FA, and further determines the molecule number for assembly with different morphologies and porosities.

To investigate the application of SM-FA in PIBs, the solubility of SM-FA-x (x = 1–7) in organic electrolyte (1.0 mol/L KPF_6 in ethylene carbonate/diethyl carbonate (EC/DEC, v/v = 1:1)) was investigated. The pristine FA and SM-FA-x (x = 1–4) were dissolved in EC/DEC, while SM-FA-x (x = 5–7) were insoluble, which can be concluded that the SM-FA assembled by disk HB mode is more stable in EC/EDC solution compared to band HB mode (Fig. 2). This may be ascribed to the fact that, in the disk HB mode, multi-locus HBs and supersized cyclized π-conjugated interactions stabilize the structure of SM-FA-x (x = 5–7) [25,26]. Considering the solubility and specific surface area of SM-FA-x (x = 5–7), the electrochemical performance of SM-FA-6 is described in the following parts. The details of SM-FA-5 and SM-FA-7 are shown in Supporting information.

To demonstrate its unique structure and enhanced chemical stability, the potential of SM-FA-x (x = 5–7) for K^+ ion storage was further examined. Cyclic voltammetry (CV) measurements

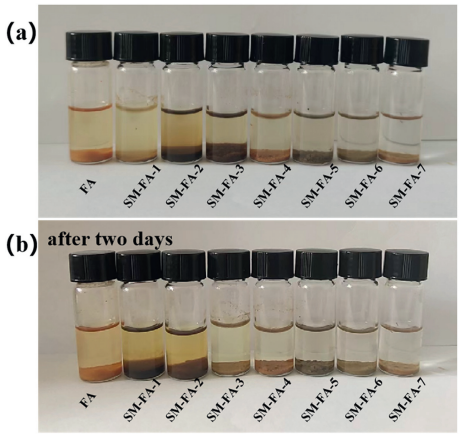

Fig. 2. (a) Solubility of FA and SM-FA-x ($x = 1–7$) in EC/DEC, and (b) the solubility after two days at room temperature.

were performed at a scan rate of 0.1 mV/s from 0.01 V to 3 V (Fig. 3a). The first cathodic scanning reveals an irreversible peak at 1.22 V, representing the formation of the solid electrolyte interface (SEI) on the surface of the electrode [27]. After the first scan, a pair of redox peaks can be observed at 0.41 and 0.57 V in both the second and third circles, and the overlapped curves indicate good reversibility of the electrodes [28]. The galvanostatic charge-discharge (GCD) analysis taken at the current density of 50 mA/g displays the detailed capacity and initial Coulombic efficiency (ICE) in Fig. 3b, the first discharge and charge capacities of SM-FA-6 are 485 and 201 mAh/g, corresponding to an ICE of 40.2%. In general, all these anodes exhibit low coulombic efficiencies in the first cycle, which are usually observed in almost all carbonaceous materials and organic materials for PIBs in the literature [29]. This phenomenon is mainly attributed to the decomposition of the electrolyte, which forms SEI film on the surface of the anode [30]. After the initial discharge, SM-FA-6 stabilizes rapidly and the coulomb efficiency is approaching to 100%. It delivers stable discharge capacity of 206 mAh/g at 50 mA/g.

To verify the rate capability of FA and SM-FA-6, the GCD curves were evaluated at different current densities (Fig. 3d). The reversible capacities of SM-FA-6 were 206, 136, 129 and 80 mAh/g when the current rate was increased from 50 mA/g to 100, 200 and 500 mA/g, respectively (Fig. 3d). When the current density returns to 50 mA/g, a 182 mAh/g capacity can be still reached. In contrast, the capacity of FA dropped from 430 mAh/g to 60.71 mAh/g after 10 cycles at 50 mA/g. After 10 cycles, the coin cells were disassembled and the color change of the separator was visually inspected (Fig. 3c). The separator of SM-FA-6 was basically intact, while the separator of FA was heavily contaminated with dissolved active material. Furthermore, the SM-FA-6 electrode based on half-cell displays an excellent cyclic stability (Fig. 3e and Fig. S6e in Supporting information), which at the current density of 50 mA/g after 1000 cycles and a high specific capacity of 187.4 mAh/g can be still retained (capacity retention rate 91%).

Electrochemical impedance spectroscopy (EIS) analysis was carried out at the 50th cycles in the fully charged and discharged states (Fig. 3f). The Nyquist plot consists of a semicircle in the high frequency region and a straight line in the low frequency region. The diameter of the semicircle is an indication of the charge transfer resistance (R_{ct}) in the electrode reaction. The slope of the line is related to the Warburg impedance (Z_w) due to potassium diffu-

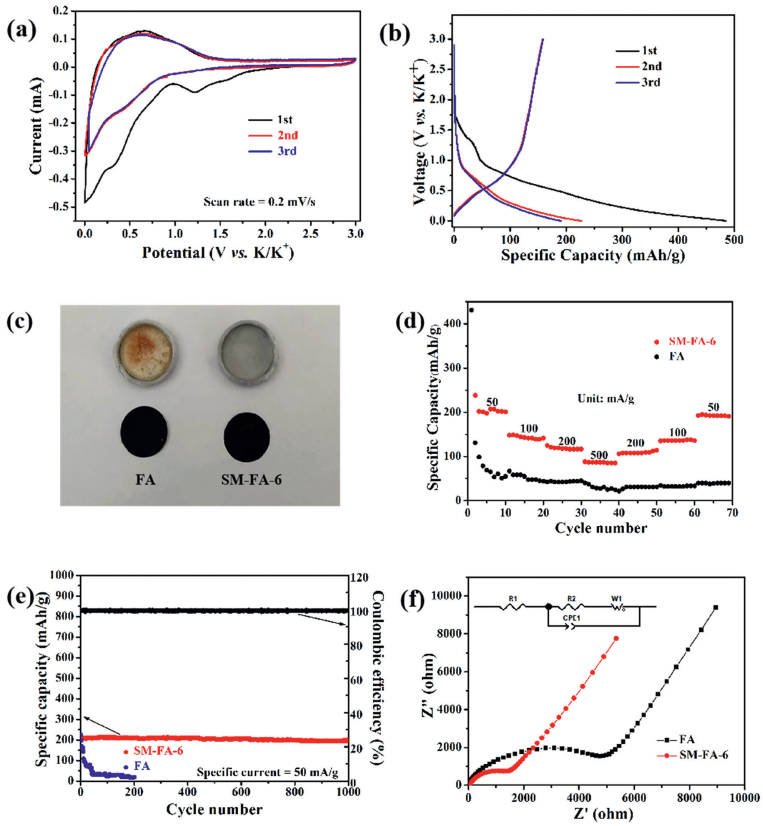

Fig. 3. Electrochemical performances of SM-FA-6 and FA for K^+ ion storage. (a) CV curves at 0.2 mV/s, (b) galvanostatic charge and discharge curves for the first 3 cycles at 50 mA/g, (c) separator membranes after 10 cycles, (d) rate performance at various current densities, (e) cycling stability at 50 mA/g, (f) Nyquist plots of the electrodes after 50 cycles.

sion [26]. By fitting the equivalent circuit, the lower value of R_{ct} for SM-FA-6 (1500 Ω) clearly indicates that the SM-FA-6 anode has a faster charge transport process than the FA (5100 Ω). The desirable performance of SM-FA-6 can be attributed to the short diffusion distances related to the ultra-thin two-dimensional geometry and the enhanced K^+ diffusion kinetics within the organic framework [31].

To investigate the electrochemical kinetics of SM-FA-6, the CV tests were carried out at different scan rates (Fig. S7a in Supporting information). The CV cycling curve of SM-FA-6 remained consistent with increasing scan rate over the range of scan rates tested, demonstrating the good stability and reversibility of K-ions storage [32]. Based on Equation: $i = av^b$, in which a and b are regulated values, when the value of b is 0.5, it advises the diffusion control process, and once the value of b reaches 1.0, it indicates the control process of surface pseudocapacitance [33]. From Fig. S8b (Supporting information), the values of b for peak I and peak II are 0.90 and 0.85, respectively. Therefore, SM-FA-6 is dominated by surface pseudocapacitance behavior. Taking a typical 5 mV/s scan as an example (Fig. S8 in Supporting information), the contribution of surface capacitance for the SM-FA-6 electrode in K-ions storage is 70.84% by calculation (Fig. S8d). It should be noted that the calculation of capacitive or diffusion percentage is rough estimation and the practical K-storage mechanism in the bulk electrode or just from the surface of the electrode is very complicated [34]. One should consider both the total capacity and the contribution ratios of diffusion or surface behaviors for the electrode materials.

To further investigate the K-ions storage mechanism of SM-FA-6, the *ex-situ* X-ray photoelectron spectroscopy (XPS) characterization was used to examine the changes of functional groups during the discharge/charge process at the interval of 0.01–3 V (Fig. 4a). As shown in Fig. 4b, the high-resolution C 1s spectra can be deconvoluted into four peaks at 283.2, 284.6, 285.7 and 288.0 eV, which is ascribed to C=C/C–C, C–N/C–O, C=N and C=O species respectively [35]. Comparing with the pristine state, the percentage of C–O group increases a lot accompanied by the converse drop of C=O component, indicating the C=O groups in the imide and carboxyl acid are converted into C–O···K species. Meanwhile, it is observed that the area ratios of C=C and C=N groups also fluctuate during the discharge/charge process, suggesting the structure variation in the conjugated pteridine unit due to the π-cation (π-K^+) interaction [17]. To further verify the reaction between C=O and K^+, the high resolution O 1s spectra is decomposed into two peaks, 531.8 eV for C–O and 533.2 eV for C=O (Fig. 4c). During potassisation, the proportion of the C–O peak increases along with the intensity decrease of C=O peak, informing that the C=O groups undergo enolization with K^+ to form C–O···K. After depotassisation, the intensity of the C–O peak decreases while C=O increased, signifying a reversible interaction between K^+ and the C=O group, coincident with the observation in C 1s spectra [36]. Moreover, two peaks at 292.6 and 295.1 eV are observed in the high resolution K 2p spectra, which can be assigned to K $2p_{3/2}$ and K $2p_{1/2}$, respectively. The intensities of these two peaks fluctuate periodically, implying the reversible interaction between K^+ and SM-FA-6 (Fig. S12 in Supporting information) [17]. Besides the experimental detection, the theoretical capacity (TC) of SM-FA-6 is also calculated and discussed. If the sole enolization reactions is considered, the calculated TC value of FA is 144 mAh/g (Fig. S13 in Supporting information). The measured TC value (206 mAh/g) is larger than 144 mAh/g, close to 210 mAh/g, and far below 241 mAh/g, suggesting that a pteridine group tends to carry one K^+ due to the statistical repulse force involved. Based on the XPS characterization and the TC calculation, an integrative storage mechanism, which combines both the general enolization reaction between C=O groups and K^+, and atypical π–K^+ interaction within the assembled conjugation framework, is schematically uncovered for K^+ storage (Fig. 4d).

To further evaluate the practical application of SM-FAs, SM-FA-6 and the PB ($K_{0.22}Fe[Fe(CN)_6]_{0.805}\cdot 4H_2O$) is used as anode and cathode respectively to assemble a full PIB [37]. The detailed electrochemical performance is exhibited in Fig. S13. Fig. S14b (Supporting information) exhibits charge/discharge curves at 100 mA/g, revealing a good reversible capacity. It is demonstrated that the fabricated PIB delivers a specific capacity of 125, 101, 80 and 61 mAh/g at the current density of 50, 100, 200, 500 mA/g, respectively (Fig. S14c in Supporting information). Moreover, an excellent cycling stability of the SM-FA-6//PB PIB is presented, in which a capacity retention rate of 89.1% is retained at a current density of 50 mA/g after 500 cycles (Fig. S14d in Supporting information), referring the possibility of the practical application of SM-FA as an anode for PIB.

In conclusion, the stable SM-FA was successfully constructed by a hydrothermal strategy and applied for potassium ion storage. Resorting to the multiple HBs, the SM-FA demonstrates a reduced solubility in carbonate-based electrolytes. As an anode for PIBs, the

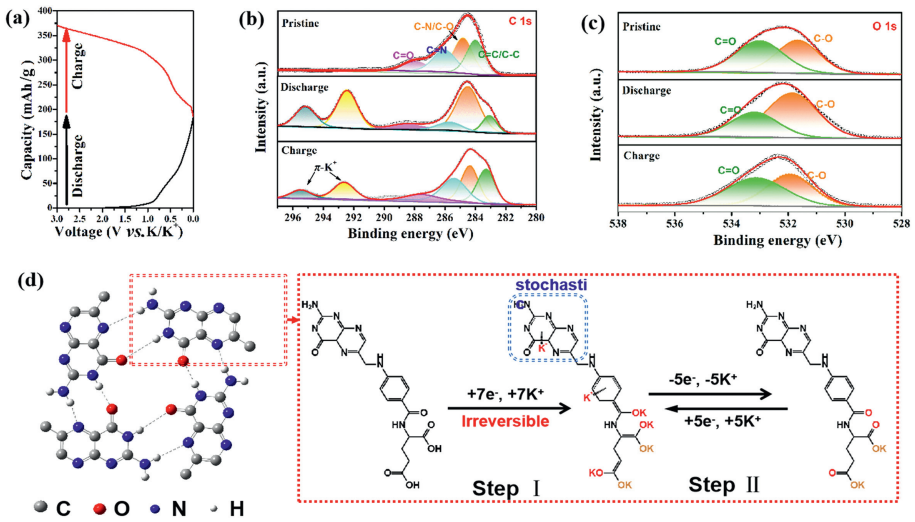

Fig. 4. (a) Typical discharge/charge curves. (b) C 1s and (c) O 1s spectra of *ex-situ* XPS spectra. (d) Proposed energy storage mechanism of SM-FA-6 and corresponding variation of molecular structure during discharge/charge process.

typical SM-FA-6 sample displays a large capacity (206 mAh/g at 50 mA/g), a favorable rate capability (77 mAh/g at 500 mA/g) and a durable stability (115.2 mAh/g after 4000 cycles at 200 mA/g). Combining with the PB cathode, the assembled PIB validates the promising application of SM-FA for K^+ storage. Impressively, the *ex-situ* XPS reveals that besides the general C=O group, the π-K^+ interaction within the conjugated pteridine groups plays an important role in the extra capacity enhancement. It is envisioned that this work not only provides a green strategy to improve the cycling stability of the organic electrodes, but also unravel the additional K^+ capacity enhancement from the π-cation interactions.

Declaration of competing interest

The authors declare that they have no known competing financial interests or personal relationships that could have appeared to influence the work reported in this paper.

Acknowledgments

This work was the financially supported by the "Western Light" Foundation of Chinese Academy of Sciences (No. 2019-XBQNXZ-A-002), the Youth Innovation Promotion Association, Chinese Academy of Sciences (No. 2019427), the Xinjiang Science Foundation for Distinguished Young Scholars (No. 2019Q004), and the Key Research and Development Projects of Xinjiang Uygur Autonomous Region (Nos. 2022B02013 and 2022B01023).

Supplementary materials

Supplementary material associated with this article can be found, in the online version, at doi:10.1016/j.cclet.2022.108095.

References

[1] T. Hosaka, K. Kubota, A.S. H.ameed, et al., Chem. Rev. 120 (2020) 6358–6466.
[2] Y. Lu, J. Chen, Nat. Rev. Chem. 4 (2020) 127–142.
[3] P. Poizot, J. Gaubicher, S. Renault, et al., Chem. Rev. 120 (2020) 6490–6557.
[4] Y. Chen, K. Fan, Y. Gao, et al., Adv. Mater. 34 (2022) 2200662.
[5] C.H. J.o, N. Voronina, Y.K. S.un, et al., Adv. Mater. 33 (2021) 2006019.
[6] Q. Pan, Y. Zheng, Z. Tong, et al., Angew. Chem. Int. Ed. 60 (2021) 11835–11840.
[7] J. Xu, S. Dou, X. Cui, et al., Energy Storage Mater. 34 (2021) 85–106.
[8] W. Liu, W. Liu, Y. Jiang, et al., Chin. Chem. Lett. 32 (2021) 1299–1308.
[9] R. Shi, L. Liu, Y. Lu, et al., Adv. Energy Mater. 11 (2020) 2002917.
[10] Q. Zhao, S. Stalin, C.Z. Zhao, et al., Nat. Rev. Mater. 5 (2020) 229–252.
[11] X. Wu, S. Qiu, Y. Liu, et al., Adv. Mater. 34 (2021) 2106876.
[12] H. Li, J. Wu, H. Li, et al., Chem. Eng. J. 430 (2022) 1–10.
[13] T. Sun, J. Xie, W. Guo, et al., Adv. Energy Mater. 10 (2020) 1904199.
[14] W. Zhu, A. Li, Z. Wang, et al., Small 17 (2021) 2006424.
[15] Y. Hu, W. Tang, Q. Yu, et al., Adv. Funct. Mater. 30 (2020) 2000675.
[16] R.B. Lin, Y. He, P. Li, et al., Chem. Soc. Rev. 48 (2019) 1362–1389.
[17] X.X. L.uo, W.H. L.i, H.J. L.iang, et al., Angew. Chem. Int. Ed. 61 (2022) e202117661.
[18] Y. Wu, X. Mao, M. Zhang, et al., Adv. Mater. 33 (2021) 2106079.
[19] P. Xiong, Y. Wu, Y. Liu, et al., Energy Environ. Sci. 13 (2020) 4834–4853.
[20] X. Zhang, T. Xiong, B. He, et al., Energy Environ. Sci. 15 (2022) 3750–3774.
[21] X. Zhang, G. Li, J. Wang, et al., ACS Appl. Mater. Interfaces 14 (2022) 27968–27978.
[22] M.R. T.uttle, S.T. D.avis, S. Zhang, ACS Energy Lett. 6 (2021) 643–649.
[23] F. Jiang, H. Ye, H. Li, et al., Chem. Commun. 54 (2018) 4971–4974.
[24] P. Xing, X. Chu, M. Ma, et al., Phys. Chem. Chem. Phys. 16 (2014) 8346–8359.
[25] T. Kato, T. Yasuda, Y. Kamikawa, et al., Chem. Commun. (2009) 729–739.
[26] Y. Hu, C. Tang, H. Li, et al., Chin. Chem. Lett. 33 (2022) 480–485.
[27] H. Wang, D. Zhai, F. Kang, Energy Environ. Sci. 13 (2020) 4583–4608.
[28] Q. Liu, A.M. R.ao, X. Han, et al., Adv. Sci. 8 (2021) 2003639.
[29] M. Zhou, P. Bai, X. Ji, et al., Adv. Mater. 33 (2021) 2003741.
[30] Q. Deng, C. Tian, Z. Luo, et al., Chem. Commun. 56 (2020) 12234–12237.
[31] T. Kato, Science 295 (2002) 2414–2418.
[32] Q. Xue, D. Li, Y. Huang, et al., J. Mater. Chem. A 6 (2018) 12559–12564.
[33] A. Yu, Q. Pan, M. Zhang, et al., Adv. Funct. Mater. 30 (2020) 2001440.
[34] J. Zhang, L. Lai, H. Wang, et al., Mater. Today Energy 21 (2021) 100747.
[35] G. Li, J. Wang, J. Chu, et al., Energy Storage Mater. 47 (2022) 1–12.
[36] X. Chen, H. Zhang, C. Ci, et al., ACS Nano 13 (2019) 3600–3607.
[37] Y. Qi, Y. Yang, Q. Hou, et al., Chin. Chem. Lett. 32 (2021) 1117–1120.